A simple model to estimate plantarflexor muscle-tendon mechanics and energetics during walking with elastic ankle exoskeletons

Gregory S. Sawicki, Nabil S. Khan

***Abstract*— *Goal:* A recent experiment demonstrated that when humans wear unpowered elastic ankle exoskeletons with intermediate spring stiffness they can reduce their metabolic energy cost to walk by ~7%. Springs that are too compliant or too stiff have little benefit. The purpose of this study was to use modeling and simulation to explore the muscle-level mechanisms for the 'sweet-spot' in stiffness during exoskeleton assisted walking. *Methods:* We developed a simple lumped, uniarticular musculoskeletal model of the plantarflexors operating in parallel with an elastic 'exo-tendon'. Using an inverse approach with constrained kinematics and kinetics, we rapidly simulated human walking over a range of exoskeleton stiffness values and examined the underlying neuromechanics and energetics of the biological plantarflexors. *Results:* Stiffer ankle exoskeleton springs resulted in larger decreases in plantarflexor muscle forces, activations and metabolic energy consumption. However, in the process of unloading the compliant biological muscle-tendon unit (MTU), the muscle fascicles (CE) experienced larger excursions that negatively impacted series elastic element (SEE) recoil that is characteristic of a tuned 'catapult mechanism'. *Conclusion:* The combination of disrupted muscle-tendon dynamics and the need to produce compensatory forces/moments to maintain overall net ankle moment invariance could explain the 'sweet spot' in metabolic performance at intermediate ankle exoskeleton stiffness. Future work will aim to provide experimental evidence to support the model predictions presented here using ultrasound imaging of muscle-level dynamics during walking with elastic ankle exoskeletons. *Significance:* Engineers must account for the muscle-level effects of exoskeleton designs in order to achieve maximal performance objectives.**

***Index Terms*—ankle exoskeleton, computer simulation, elastic energy storage, energetics, Hill-type muscle model, metabolic cost, muscle-tendon dynamics, plantarflexors, human walking**

Manuscript received August 14, 2015. This work was supported by the US-Israel Binational Science Foundation Grant #2011152 and the National Institute of Nursing Research of the National Institutes of Health under Grant #R01NR014756, both to G.S.S.

G.S. Sawicki, Ph.D. is with the Joint Department of Biomedical Engineering-North Carolina State University and the University of North Carolina-Chapel Hill, Raleigh, NC 27695 USA (e-mail: greg_sawicki@ ncsu.edu).

N. S. Khan, M.S. was a graduate student in the Joint Department of BME-NC State and the UNC-Chapel Hill, Raleigh, NC 27695 USA. He is now an Embedded Software Engineer at Anuva Innovations, Inc., a medical device development company in the Research Triangle Park, NC USA (e-mail: Nabilsalihkhan@ gmail.com).

I. Introduction

HUMAN walking [4], hopping [5], and running [6] all exhibit compliant dynamics that can be captured by simple spring-mass models. In essence, the lower-limb is able to compress and recoil elastically with stiffness that arises from the combination of passive, non-linear material properties of the muscles and series elastic connective tissues, and active neuromuscular control. During locomotion, 'springy-limbs' enable a number of elastic mechanisms that are exploited to improve performance. For example, properly timed stretch and recoil of series elastic tissues can be used to enhance muscle power output during acceleration, attenuate muscle power requirements during deceleration, or conserve mechanical and metabolic energy during steady speed locomotion [7].

The range of performance benefits afforded by compliant limbs in humans and animals has inspired wearable exoskeletons that may have applications in both gait rehabilitation and augmentation. Recently, a number of lower-limb exoskeletons have been developed that use elastic elements (*i.e.*, springs and clutches) in parallel with the limb to strategically store and return energy and help power locomotion [8-15]. Physiological measurements in studies of vertical hopping in elastic exoskeletons spanning the whole limb [9] the knee joint [14] and the ankle joint [10, 12, 20] indicate performance benefits that include reduced muscle activity, reduced biological limb/joint stiffness and mechanical power output, and reduced metabolic energy cost of the user. These studies of simple movements like vertical hopping have paved the way for the continued development and implementation of elastic exoskeletons to improve user performance during human walking and running gaits.

During human walking, the majority of mechanical power comes from the ankle plantarflexors [21]. Furthermore, approximately half of the requisite mechanical power output at the ankle comes from elastic recoil of the Achilles' tendon at 'push-off' [22]. Given the plantarflexors' primary role in forward propulsion [23] and the significant elastic mechanism afforded by their compliant muscle-tendon architecture, the ankle joint seems to be a logical site for a passive elastic exoskeleton that can improve human walking performance.

We have recently developed a novel, passive elastic ankle

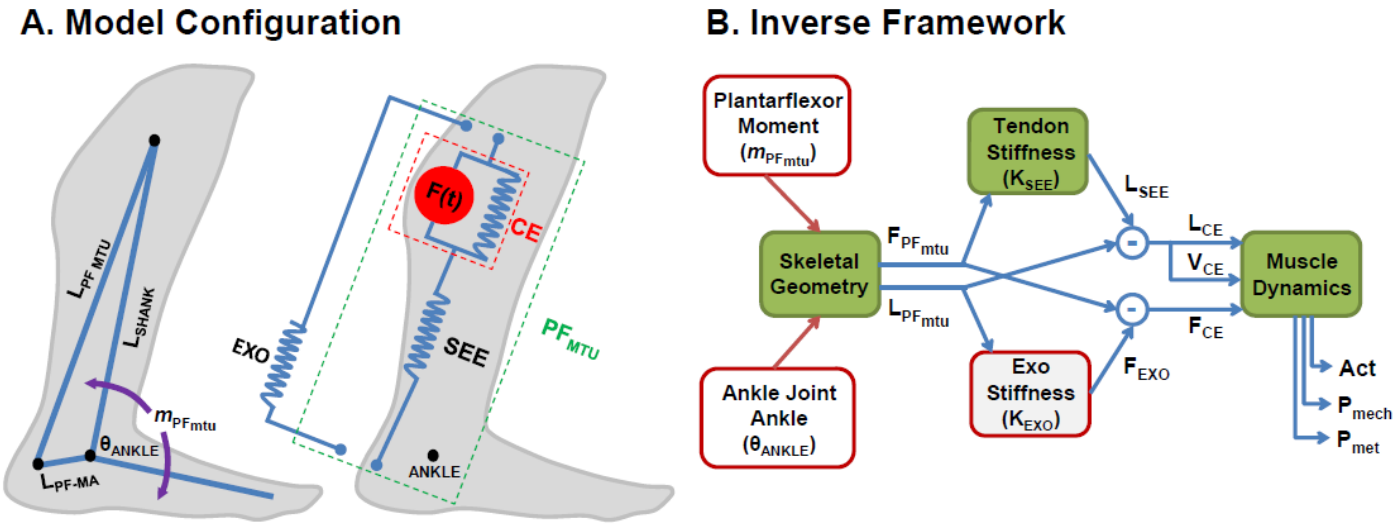

Fig. 1. (A) Modeling schematic. We modeled the combined triceps surae (soleus and gastrocnemius muscles) as a single lumped uniarticular plantarflexor (PF_{mtu}) attached along the shank L_{SHANK} to the calcaneus with length $L_{PF_{mtu}}$ and moment arm L_{PF-MA} (left). The lumped PF_{mtu} generated force according to a Hill-type muscle-tendon model with a muscle contractile element (CE) comprising active (F(t), red) and passive (blue parallel spring) components and a series elastic component (SEE) representing the Achilles' tendon and aponeurosis. We modeled a passive elastic ankle exoskeleton (EXO) as a spring in parallel with the PF_{MTU} and acting through the same moment arm L_{PF-MA} (right). (B) Block diagram of computational flow in the inverse modeling framework used to simulate changes in muscle-level dynamics during walking with exoskeletons of varying spring stiffness, K_{EXO}. First, using the defined skeletal geometry, the plantar flexor moment, $m_{PF_{mtu}}$ and ankle joint angle, θ_{ANKLE} from normal walking at 1.25 m/s were converted to a plantar flexor force, $F_{PF_{mtu}}$ and plantar flexor length, $L_{PF_{mtu}}$, respectively. Then, we used the series elastic element stiffness, K_{SEE} to compute SEE length, L_{SEE}; and the exoskeleton stiffness, K_{EXO} to compute exoskeleton force, F_{EXO}. Next, we could use subtraction to define the force (F_{CE}), length (L_{CE}), and velocity (V_{CE}), of the muscle. Finally, these values were used along with models of muscle force production and metabolic energy use to compute muscle activation (Act), mechanical power output (P_{mech}) and metabolic power output (P_{met}).

exoskeleton that can store and return energy during the stance phase while allowing free ankle rotation during the swing phase of walking [8, 24, 25]. The key feature in the design is a rotary clutch that uses a ratchet and pawl configuration and two timing pins set to engage and disengage the exoskeleton spring at set ankle joint angles. The exoskeleton spring is engaged when the first timing pin pushes the pawl onto the ratchet at terminal swing, where the ankle dorsiflexes just prior to heel strike. This enables the spring to store and return elastic energy during stance. Then, once the ankle reaches extreme plantarflexion, after the foot is off the ground, a second timing pin pushes the pawl off of the ratchet, allowing the user to freely rotate their foot without interference from the exoskeleton spring. This exoskeleton design is simple, lightweight (<500 g), and requires no electronics or battery, making it a low cost option for gait assistance. We have recently shown that users can use this unpowered exoskeleton to reduce their metabolic cost of walking by ~7% below normal walking, but only when the exoskeleton spring (*i.e.*, 'exo-tendon') is not too compliant and not too stiff [25]. The reasons behind the existence of a 'sweet-spot' for ankle exoskeleton stiffness remain unresolved, principally because it is difficult to experimentally observe muscle-level effects of exoskeleton mechanical assistance.

The goal of this study was to develop and employ a simple *in silico* modeling tool to aid in the muscle-level understanding of the effects of increasing elastic ankle exoskeleton stiffness on underlying plantarflexor muscle-tendon mechanics and energetics during walking. Humans tend to reduce their biological ankle moment contribution in order to maintain consistent overall ankle joint kinetics during walking with ankle exoskeletons [11, 25, 29, 30]. In line with this adaptive behavior, it follows that higher exoskeleton stiffness should result in increased unloading of biological muscle-tendons and larger reductions in the metabolic cost of plantarflexion during walking. On the other hand, if elastic ankle exoskeletons get *too stiff*, costly compensations might arise elsewhere in the lower-limb [31] or locally at the ankle in antagonistic muscle groups (*e.g.*, tibialis anterior) to maintain steady gait mechanics. Furthermore, at the muscle-tendon level, increasing ankle exoskeleton stiffness could disrupt the normal 'catapult mechanism' exhibited by the ankle plantarflexors. That is, as parallel spring stiffness increases and the exoskeleton takes over more and more of the plantarflexor moment, the Achilles' tendon should undergo less stretch requiring larger excursions of the muscles fascicles in series. Higher muscle shortening velocities are more metabolically costly. Thus, despite lower muscle force/moment requirements, it is possible that unfavorable shifts in force–length or force-velocity operating point (*e.g.*, higher shorting velocities) could increase metabolic energy requirements in the plantarflexor muscles and offset the potential benefit of increased assistance from elastic ankle exoskeletons [20, 32, 33].

To begin to resolve the reasons behind the 'sweet-spot' in ankle exoskeleton stiffness, we built a strategically simple musculoskeletal model of a passive elastic ankle exoskeleton working in parallel with the human ankle plantarflexors (Figure 1A.). We first used experimental kinematic and kinetic data from normal walking without exoskeletons at 1.25 m/s, to identify the best set of morphological parameters and neural activation ($\vec{M}_{bio}$) that generated 'human-like' ankle

TABLE I: BASELINE MODEL PARAMETERS AND $\vec{M}_{bio}$ SOLUTION

Parameter	Value (units) (Norm.)	Source/Details
Body Mass	70 kg	Average mass of subjects from experimental data set for walking at 1.25 m/s [2]. Within 1 SD of average subject mass from Ward et al. (82.7 ± 15.2 kg) [3].
Body Height	1.70 m	Average height of subjects from experimental data set for walking at 1.25 m/s [2]. Within 1 SD of average subject height from Ward et al. (168.4 ± 9.3 m) [3].
Shank Length, L_{SHANK}	0.400 m	Set 0.03 m greater than tibial length from Ward et al. (37.1 ± 2.2 cm) [3] to include distance to femoral condyles.
$F_{CE_{MAX}}$	6000 N	Similar to approximations for soleus + med. and lat. gastrocnemius muscles used by Arnold et al. (5500.3 N) [16] and others [17-19].
$V_{CE_{MAX}}$	0.326 m/s (8.24 x L_{CE_0})	Based on values for soleus and combined gastrocnemius reported by Geyer et al. [19] and scaled using physiological cross section (PCSA) data from Ward et al. [3]
$L_{CE_0}/L_{PF_{mtu_0}}$	0.108 (unitless)	Based on fascicle lengths for soleus, med. gastrocnemius and lat. gastrocnemius reported in Ward et al. [3] and tendon slack lengths reported in Arnold et al. [16] and scaled using physiological cross section (PCSA) data from Ward et al. [3]
$\boldsymbol{L_{PF_{mtu_0}}}$	**0.366 m (0.92 x L_{SHANK})**	
$\boldsymbol{L_{CE_0}}$	**0.040 m (0.10 x L_{SHANK})**	These values (**in bold**) were all obtained using an optimization to find the morphology that would minimize error between the modeled and measured plantarflexor moment based on inverse dynamics analysis of human walking data collected at 1.25 m/s. See text for details
$\boldsymbol{L_{SEE_0}}$	**0.326 m (0.82 x L_{SHANK})**	
$\boldsymbol{K_{SEE}}$	**315.4 N/mm**	The stiffness of the SEE that resulted in the best match of model and experimental plantarflexor moment is consistent with values reported for the Achilles' tendon in the literature from both models (375.6 N/mm) [18] and experiments (188 N/mm-805 N/mm) [26-28].

*Parameters are all defined in more detail within the text. **Bold** indicates a parameter set using optimization to match model and experimental data ($\vec{M}_{bio}$); un-bold indicates a parameter based on values taken from literature.

neuromechanics and energetics (*e.g.*, [18]). Then with $\vec{M}_{bio}$ as baseline, and an inverse framework (Figure 1B) we performed computer simulations to estimate how changes in ankle exoskeleton stiffness in parallel with the plantarflexors would impact the underlying biological muscle-level neuromechanics and energetics.

II. METHODS

A. Model Composition.

We constructed a simplified model of the human triceps surae using a single, lumped, uniarticular ankle plantarflexor (PF) muscle-tendon unit (MTU). Within the MTU there was a Hill-type contractile element (CE), representing the muscle fascicles, and a series elastic element (SEE), representing tendonous tisses (*i.e.*, Achilles' tendon and aponeuroses) [34] (Figure 1A). The extended model also included a spring in parallel with and operating through the same moment arm as the biological MTU (Figure 1A) in order to capture the dynamics of an elastic ankle exoskeleton (EXO). More details describing mathematical relations used to model components of the MTU are provided in the online Supplementary Materials.

B. Setting Model Parameter Values.

We set model parameters describing attachment geometry, MTU morphology and muscle (CE) and tendon (SEE) force production based on the latest anatomical and physiological data from the literature (*e.g.*, [3, 16]) as well as computer optimization (*e.g.*, [18]) to match model outputs to baseline experimental walking data (Table 1, un-bold and bold respectively). We termed this 'baseline' lumped muscle model without an exoskeleton the $\vec{M}_{bio}$ parameter configuration. More details on how we set parameters are provided in the online Supplementary Materials.

C. Extending the Model to Include an Elastic Ankle Exoskeleton.

We modified the 'baseline' lumped muscle model configured to $\vec{M}_{bio}$ (Table 1, bold; see Supp. Materials for more details) to include a passive elastic exoskeleton (EXO), represented by an additional passive elastic element operating in parallel with and along the same line of action as the lumped plantarflexor MTU (Figure 1A). In this configuration, the exoskeleton spring (*i.e.*, exo-tendon) operated through the same moment arm (~4.1 cm) as the plantarflexor MTU throughout the stride- a simplification that is convenient for tying the exoskeleton back to parameters of the biological MTU (*i.e.*, K_{SEE}) and allows simple conversion to equivalent effective rotational stiffness values– both features that facilitate broad generalization to devices with varying geometries.

We modeled the mechanical action of EXO based on the passive ankle exoskeleton developed by Wiggin and colleagues which utilizes a clutch to strategically engage and disengage a coil tension spring according to kinematic cues based on ankle angle [8, 24, 25]. The length of the EXO spring always exactly tracked the length of the lumped plantarflexor MTU, $L_{PF_{mtu}}$ (Equation 1).

$$L_{EXO}(t) = L_{PF_{mtu}}(t) \quad (1)$$

To model the function of the clutch, the effective slack length of the EXO spring, L_{EXO_0}, was set to the MTU length at

which the ankle angle transitioned from plantarflexion into dorsiflexion shortly after heel strike (Equation 2).

$$L_{EXO_0} = L_{PF_{mtu}}(t*) \text{ where } \frac{d\theta_{ankle}}{dt}(t*) = 0 \text{ and } \frac{d^2\theta_{ankle}}{dt^2}(t*) > 0 \quad (2)$$

After this point, the EXO spring stored and released energy until the second transition from plantarflexion to dorsiflexion, at which time EXO force generation capability was terminated (*i.e.*, shortly before swing). EXO force generation was modeled using a hookean spring with linear stiffness, K_{EXO} (Equation 3).

$$F_{EXO}(t) = K_{EXO} \times (L_{EXO}(t) - L_{EXO_0}), L_{EXO} > L_{EXO_0}$$
$$F_{EXO}(t) = 0, \quad L_{EXO} < L_{EXO_0} \quad (3)$$

D. An Inverse Approach to Simulate Walking with Ankle Exoskeletons Over a Range of Stiffnesses.

With the EXO component of the model defined and parameters of the lumped biological MTU set to $\vec{M}_{bio}$ we sought to examine changes in mechanics and energetics of the biological MTU during walking with exoskeleton springs ranging 0% to 100% of the MTU series elastic stiffness, K_{SEE} = 315.4 N/mm. This yielded equivalent exoskeleton rotational stiffness values ranging from 0 N-m/rad (0 N-m/deg) up to 526.7 N-m/rad (9.19 N-m/deg), a value similar to that observed for the ankle joint in late stance during normal walking at 1.25 m/s [35] .

For these simulations we used an inverse approach (Figure 1B) that conserved ankle joint angle, θ_{ANKLE}, and by extension the lumped plantar flexor muscle-tendon unit length change $L_{PF_{mtu}}$(*i.e.*, kinematics) as well as the *total* plantarflexor moment profile $m_{PF_{total}}$ (*i.e.*, kinetics), generated by the $\vec{M}_{bio}$ solution. First,F_{EXO} was calculated for each point in the stride according to Equation 3 and then converted to m_{EXO}, assuming for simplicity that it followed the same line of action as the plantarflexors by applying a moment arm computed from the model's skeletal geometry (~4.1 cm on average). Next we computed the moment generated by the biological MTUs, $m_{PF_{mtu}}$ (plantarflexors) and $m_{DF_{mtu}}$(dorsiflexors) using Equation 4.

$$m_{PF_{mtu}}(\text{t}) = m_{PF_{total}}(t) - m_{EXO}(t) \text{ when } m_{EXO} < m_{PF_{total}} \text{ and } m_{PF_{mtu}} = 0$$
$$m_{DF_{mtu}}(\text{t}) = m_{EXO}(t) - m_{PF_{total}}(t) \text{ when } m_{EXO} >= m_{PF_{total}} \quad (4)$$

In cases where m_{EXO} was greater than $m_{PF_{total}}$ (*i.e.*, $m_{PF_{mtu}} < 0$) we set $m_{PF_{mtu}} = 0$ and assumed that the excess exoskeleton moment ($m_{EXO} - m_{PF_{total}}$) would be compensated for by a moment from the antagonist muscle compartment (*i.e.*, dorsiflexors), $m_{DF_{mtu}}$ to conserve the net ankle joint moment (see also Section E3 on Compensatory metabolic cost.)

Next, to get at the biological muscle-tendon dynamics we converted $m_{PF_{total}}$ to $F_{PF_{total}}$, again using a moment arm computed from the model's skeletal geometry (~4.1 cm on average). Given that all elements of the plantarflexor (PF) MTU are in series

$$F_{PF_{mtu}}(t) = F_{SEE}(t) = F_{CE}(t) \quad (5)$$

we could use $F_{SEE}(t)$ (Equation 5) and K_{SEE} to compute $L_{SEE}(t)$ (Equations S7, S8). $L_{SEE}(t)$ was then subtracted from $L_{PF_{mtu}}(t)$ to determine the L_{CE}(t) profile (Equation S9). With $L_{CE}(t)$ defined for all points during the stride, we could compute a time derivative to obtain the muscle fascicle (CE) velocity, $V_{CE}(t)$. Finally, we could use our model for CE force to back calculate the muscle activation $\alpha(t)$ over the stride given the known $F_{CE}(t)$, $L_{CE}(t)$ and $V_{CE}(t)$ (Equation S1). At this point the forces, lengths and velocities of the EXO, MTU, SEE and CE, as well as the activation of the CE were all known and available to assess the *muscle-level* mechanical and energetic performance of a given exoskeleton stiffness during assisted walking.

E. Assessment Metrics for Quantifying Exoskeleton Performance at the Muscle Level.

To evaluate the effects of different exoskeleton springs on underlying plantarflexor mechanics and energetics we calculated mechanical power of the MTU and its elements (CE and SEE) as well as the metabolic power of the CE.

E.1. Mechanical power.

For a given element (MTU, CE or SEE), mechanical power (in watts), $P_{Mech}(t)$, was calculated by taking the product of force and velocity at each time point over the stride (Equation 6).

$$P_{Mech}(t) = F_{element}(t) * V_{element}(t) \quad (6)$$

The total positive mechanical work (in joules) performed by each element over the stride was also calculated by integrating the mechanical power curves over the stride only in regions with $P_{Mech} > 0$ (Equation 7).

$$W^+_{Mech} = \int P^+_{Mech}(t) * dt \quad (7)$$

E.2. Metabolic power.

A mathematical model based on isolated muscle experiments was used to estimate the metabolic energy expenditure by the lumped plantarflexor muscles (CE) over the stride [36, 37] (Equations 8-11). The heat generated in each state of the muscle contraction, including maintenance, shortening, resting, and activation, are represented in this

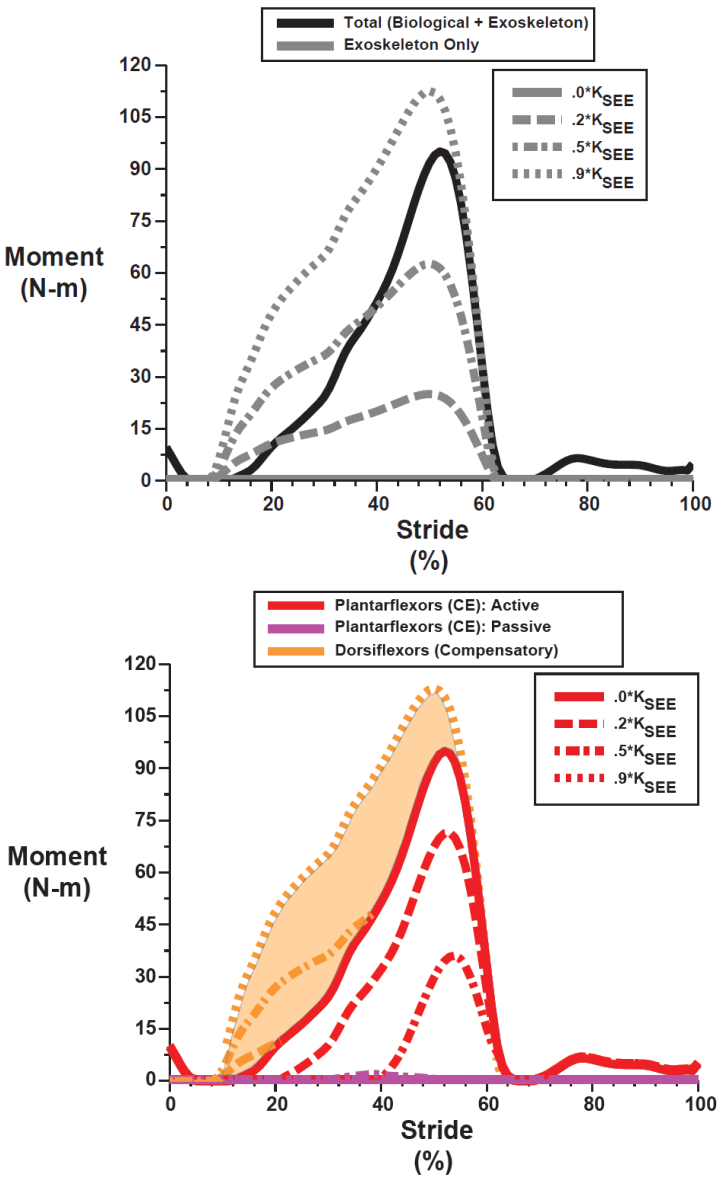

Fig. 2. The total contribution to ankle joint moment from the lumped plantarflexors and the elastic ankle exoskeleton (biological +exoskeleton) (*Top*, black) and the moment generated by the exoskeleton (exoskeleton only) (*Top*, gray) over a walking stride from heel strike (0%) to heel strike (100%) for different exoskeleton spring stiffnesses. The total moment is always the same because we constrained the model to follow the plantarflexor contribution to net ankle moment during unassisted walking (*i.e.*, $\vec{M}_{bio}$ solution) in *all* conditions. The active (*Bottom*, red) and passive (*Bottom*, purple) lumped plantarflexor muscle (CE) moment (*i.e.*, biological only) for different exoskeleton spring stiffnesses. For exoskeleton springs >0.2 K_{SEE} the exoskeleton moment exceeds the total moment and necessitates a compensatory antagonist moment from dorsiflexors (*Bottom*, shaded area=difference between orange curves and solid red curve) to maintain an invariant net ankle moment. Curves are plotted for exoskeleton stiffness values ranging from 0.2 K_{SEE} (~105 N-m/rad) to 0.9 K_{SEE} (~474 N-m/rad).

calculation. The metabolic power (in watts), $P_{Met}(t)$ is given as:

$$P_{Met}(t) = \alpha(t) * F_{CE_{MAX}} * V_{CE_{MAX}} * f_{met}(\widetilde{V_{CE}}(t)) \quad (8)$$

Where $f_{met}(\widetilde{V_{CE}})$ represents empirically based heat measures that have been related to muscle velocity [36] (Equations 9, 10).

$$f_{met}\left(\widetilde{V_{CE}}(t)\right) = .23 - .16e^{-8\widetilde{V_{CE}}};\ \widetilde{V_{CE}} \geq 0 \quad (9)$$

$$f_{met}\left(\widetilde{V_{CE}}(t)\right) = .01 - .11\widetilde{V_{CE}} + .06e^{23\widetilde{V_{CE}}};\ \widetilde{V_{CE}} < 0 \quad (10)$$

Total metabolic work (in joules) expended over a stride was calculated by integrating the metabolic power curves (Equation 11).

$$W_{Met} = \int P_{Met}(t) * dt \quad (11)$$

E.3. Compensatory metabolic cost.

A compensatory metabolic cost was also calculated for K_{EXO} values in which exoskeleton forces/moments exceeded total plantarflexor forces/moments and resulted in a compensatory moment from the antagonist muscle compartment (*i.e.*, dorsiflexors), $m_{DF_{mtu}}$ per Equation 4. First we calculated the stride average metabolic cost per unit moment, C (in J/N-m) for the plantarflexors in the $\vec{M}_{bio}$ solution (*i.e.*, the case with no exoskeleton included) (Equation 12).

$$C = \frac{\int P_{Met}(t) * dt}{\int m_{PF_{mtu}}(t) * dt} \quad (12)$$

Then, to compute the compensatory metabolic cost (in joules) we integrated and scaled the compensatory dorsiflexor moment m_{DF} using the constant C (Equation 13).

$$W_{MetComp} = C * \int m_{DF}(t) * dt \quad (13)$$

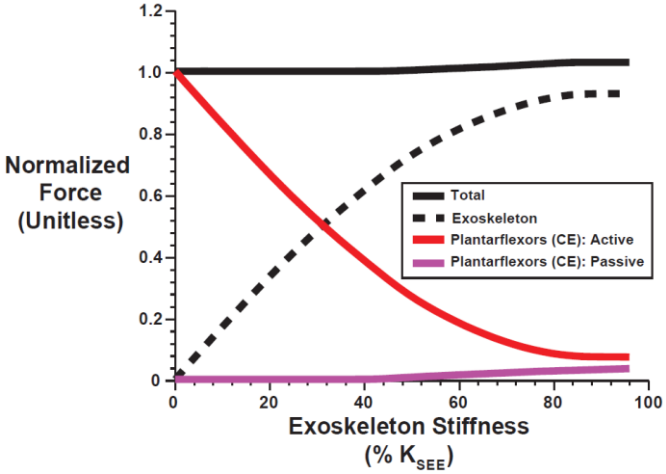

Fig. 3. Peak force versus exoskeleton spring stiffness for the total = exoskeleton + lumped plantarflexors (solid black), exoskeleton only (dashed black), and the active (solid red) and passive (solid purple) elements of the lumped plantarflexor muscles (CE). For each exoskeleton stiffness all forces are normalized to the peak total force (~3200 N) without an exoskeleton. Exoskeleton spring stiffness of 100% K_{SEE} is equivalent to ~527 N-m/rad.

III. Results

Exoskeletons with increasing stiffness developed higher and higher forces/moments over the period from ~10% to 60% of

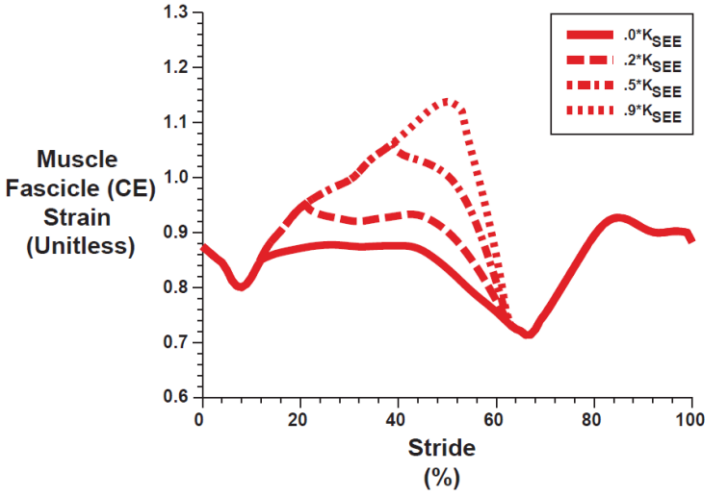

Fig. 4. Lumped plantarflexor muscle fascicle (CE) strain over a walking stride from heel strike (0%) to heel strike (100%) for different exoskeleton spring stiffnesses. The solid red line is the fascicle strain pattern taken from Rubenson et al [1] for $\vec{M}_{bio}$ solution. Curves are plotted for exoskeleton stiffness values ranging from 0.2 K_{SEE} (~105 N-m/rad) to 0.9 K_{SEE} (~474 N-m/rad).

the walking stride (Figure 2, top). Because the total exoskeleton + biological plantarflexor moment was fixed in all conditions (*i.e.*, invariant net ankle joint moment constraint), as the exoskeleton contribution to the total moment increased, the moment generated by lumped plantar flexor muscle forces (CE) systematically decreased (Figure 2, bottom; Figure 3). For the highest exoskeleton stiffnesses (*e.g.*, 0.9 K_{SEE}), the exoskeleton moment greatly exceeded the lumped plantarflexor moment necessary to maintain an invariant net ankle moment, especially early in the stride cycle. In these cases, a compensatory moment from antagonist muscles (*e.g.*, dorsiflexors) was needed to maintain the net ankle force/moment from walking without an exoskeleton (Figure 2, bottom). In addition, for stiffnesses above ~0.5 K_{SEE} (263 N-m/rad) the lumped plantarflexor muscle (CE) produced some passive force/moment (Figure 2, bottom; Figure 3).

Lumped plantarflexor muscle fascicles (CE) underwent larger excursions during stance phase (~10-60% stride) with increasing exoskeleton spring stiffness (Figure 4). Because the ankle joint angle profile was conserved across all conditions, increasing exoskeleton forces served to reduce the force and strain in the SEE which, in turn, resulted in increased CE length changes (and CE velocities) with increasing exoskeleton stiffness. In fact, L_{CE} surpassed L_{CE_0} (strain > 1.0) for K_{EXO} > ~0.5 K_{SEE}, and resulted in passive force generation. CE strain values reached ~1.15 for the stiffest exoskeleton springs.

As exoskeleton spring stiffness (K_{EXO}) increased, mechanical power/work generated by lumped plantarflexor muscle-tendon unit (MTU) decreased linearly due to systematic decreases in biological forces/moments (Figure 5, top; Figure 6). As expected, the power/work performed by the CE was approximately equal in magnitude to the power/work performed by the SEE for the condition without an exoskeleton. As K_{EXO} increased, the mechanical power/work generated by the muscle fascicles (CE) and series elastic tissues (SEE) both decreased, but the SEE well outpaced the CE leaving the CE as the dominant contributor to overall MTU power/work for exoskeletons with K_{EXO} > ~0.1 K_{SEE} (Figure 6). In fact, CE power/work did not decrease for K_{EXO} < ~0.2 K_{EXO} (~105 N-m/rad), as reduced CE forces traded-off with increased CE velocities/excursions (Figure 4) keeping CE power/work relatively constant. For K_{EXO} > 0.2 reductions in force began to dominate increases in velocity and CE power/work begin to sharply decline (Figure 6).

Lumped plantarflexor muscle (CE) activation and metabolic power/work both decreased with increasing exoskeleton stiffness (K_{EXO}) (Figure 7). Metabolic cost decreased more slowly than muscle activation with increasing exoskeleton stiffness (Figure 7, bottom-left) because the higher CE velocities associated with stiffer exoskeleton springs required more activation to achieve similar force levels. That is, with higher exoskeleton spring stiffness, CE force/unit activation decreases due to unfavorable force-velocity effects. Although increasing K_{EXO} sharply reduced the metabolic cost of the lumped plantarflexors, the metabolic cost of compensatory forces/moments needed to maintain an invariant net ankle moment sharply increased with increasing K_{EXO} (Figure 7, bottom-right). As a result, the total metabolic cost had a minimum at K_{EXO} = ~0.7 K_{EXO} (~369 N-m/rad) and was ~30% lower than the cost of ankle muscle activity for normal walking without exoskeletons.

IV. Discussion

The goal of this study was to employ a strategically simple musculoskeletal model of an elastic ankle exoskeleton working in parallel with the biological plantarflexors to determine how exoskeleton stiffness would influence the neuromechanics and energetics of the underlying muscle-tendon units during walking. We hypothesized that increasing exoskeleton stiffness would result in (1) increased unloading of biological muscle-tendons and larger reductions in the metabolic cost of the plantarflexors during walking. Furthermore, we surmised that if exoskeletons got *too* stiff, (2) costly compensations might arise in other muscles in order to maintain steady gait mechanics. Finally, at the muscle-tendon level, we hypothesized that (3) despite lower biological force/moment requirements due to exoskeleton assistance, it was possible that unfavorable changes in muscle operating length and/or higher muscle shortening velocities due to a disrupted 'catapult mechanism' early in the stance phase of the stride could increase metabolic energy requirements in the plantarflexor muscles and offset some of the potential benefit of increased assistance from elastic ankle exoskeletons. Our modeling results support all of these hypotheses and suggest potential muscle-level mechanisms behind the recently observed 'sweet spot' in elastic ankle exoskeleton stiffness [25] that must now be confirmed with follow-up experiments using ultrasound imaging.

As expected, stiffer ankle exoskeleton springs resulted in larger decreases in plantarflexor metabolic energy consumption. Humans seem to employ a motor control

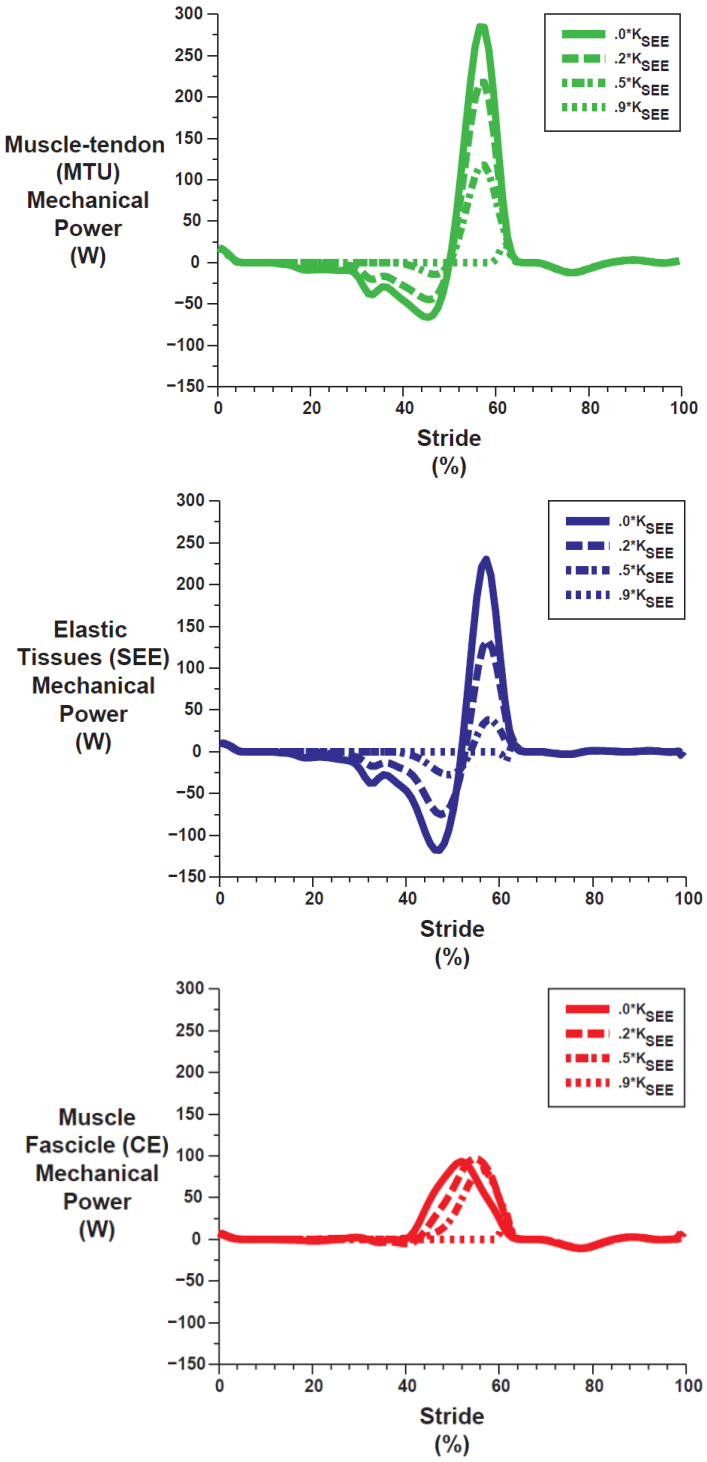

Fig. 5. Mechanical power over a walking stride from heel strike (0%) to heel strike (100%) for the lumped plantarflexor muscle-tendon unit (MTU) (*Top*, green); elastic tissues (SEE) (*Middle*, blue) and muscle fascicles (CE) (*Bottom*, red). Curves with varying line types represent different exoskeleton stiffness values ranging from no exoskeleton (bold) up 0.9 K_{SEE} (~474 N-m/rad).

strategy in order to maintain relatively invariant net ankle joint moments during locomotion with mechanical assistance from ankle exoskeletal devices [10-12, 15, 20, 25, 29, 30]. To capture the phenomenon of kinetic invariance in humans, we employed a modeling framework that enforced both the ankle angle and plantarflexor contribution to net ankle joint moment

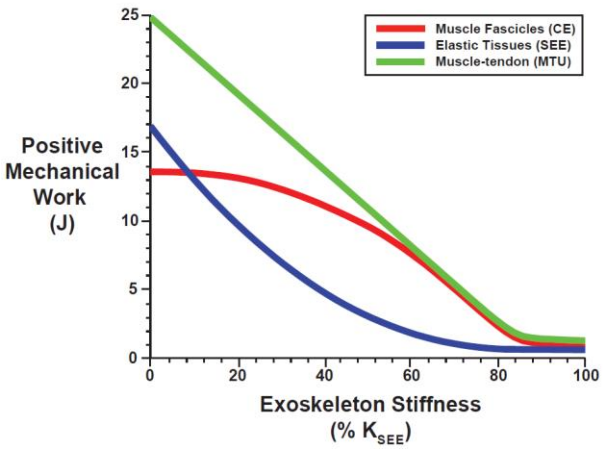

Fig. 6. Positive mechanical work versus exoskeleton spring stiffness for the lumped plantarflexor muscle fascicles (CE) (red), elastic tissues (SEE) (blue), and muscle-tendon unit (MTU) (green). Exoskeleton spring stiffness of 100% K_{SEE} is equivalent to ~527 N-m/rad.

using experimental data from normal walking at 1.25 m/s. Not surprisingly, solutions with kinetic invariance demonstrated that increasing K_{EXO} yields a clear trade-off between exoskeleton and biological muscle forces, with a ~50/50% sharing at K_{EXO} = ~0.3 K_{SEE} (~158 N-m/rad = 2.8 N-m/deg) (Figure 3). In addition, solutions with higher K_{EXO} required muscle activation with lesser magnitude *and* later onset (Figure 7, top left), a result consistent with recent experimental data showing decreases in soleus activity that are more pronounced with higher exoskeleton springs stiffness [25]. We note, without this timing shift, the lumped plantarflexor muscles (CE) would have produced unnecessary forces/moments between ~10% and 60% of the stride when exoskeleton assistance m_{EXO} was already sufficient (Figure 2). Thus, in line with our hypothesis (1), as the biological force/moment requirement declined with increasing K_{EXO}, so did muscle activation, which was the main driver of metabolic cost (Figure 7),

Metabolic cost of the plantarflexors reached a minimum value of ~11% of the value during unassisted walking (50.3 J *0.11 = 5.5 J per leg) with a K_{EXO} of ~0.8 K_{SEE} (~421N-m/rad = 7.4 N-m/deg) (Figure 7, bottom-right). But, is more necessarily better when it comes to ankle exoskeleton stiffness selection [25, 33, 38] ? Interestingly, in our model, assisting with a $K_{EXO} \geq$ ~0.5 K_{SEE} (263 N-m/rad) began to induce passive stretch in the muscle fascicles (CE) and thus a passive muscle moment contribution. While relying more on passive contributions to muscle force could have metabolic benefit, it also elicits an unavoidable deviation in the ankle force/moment profile from normal walking (Figure 2, 3). Thus, due to shifts in the operating point of underlying muscles to longer lengths (Figure 4), perfectly conserving the $m_{PF_{total}}$ may become increasingly difficult, and could be a factor that limits performance for exoskeletons employing high parallel stiffness [11, 25, 31].

If humans choose to move with very strict ankle moment invariance, our model suggests that they may reject exoskeletons with stiffness ≥ 0.5 K_{SEE} (or ~50-60% of normal ankle joint rotational stiffness during walking at 1.25 m/s

[35]), where passive forces in plantarflexors are unavoidable. This could severely limit the potential for metabolic savings to only ~60% of the total plantarflexor contribution or ~15% overall [39]. Solutions with $K_{EXO} \geq 0.5\ K_{SEE}$ (263 N-m/rad) begin to significantly produce excess exoskeleton forces/moments early in the stance phase (Figure 2). To maintain net ankle moment invariance, these excess moments would need to be countered by significant antagonist moments coming from ankle dorsiflexors or adjustments in posture, both of which would likely incur a compensatory metabolic cost (Figure 7, lower-right). Thus, a 15% reduction in overall metabolic cost of walking seems a high end estimate.

Interestingly, when adding in our estimate for the metabolic cost of compensatory force/moment of ankle antagonists (*i.e.*, dorsiflexors), our model predicts a broad 'sweet-spot' between K_{EXO}= 0.6 and 0.8 K_{SEE} (~316-420 N-m/rad) with a net metabolic benefit of ~30% for the ankle plantarflexors. Using Umberger's estimate that plantarflexors account for ~27% of the total metabolic cost of walking [39, 40], this is equivalent to an overall reduction in the metabolic cost of walking of ~8% and falls very near the measured value in Collins et al. [25], albeit at a higher range of exoskeleton stiffness. Collins et al. found the 'sweet-spot' at 180 N-m/rad, about half the stiffness for the metabolic minimum reported here. The mismatch is likely due to the very rudimentary approach we took to the compensatory metabolic cost in this study, which assumed dorsiflexors and plantarflexors have the same metabolic cost per unit moment (C in Equation 13) and did not account for the metabolic cost of compensation elsewhere in the body (*e.g.*, increased knee flexor moments).

Despite the mismatch in the 'sweet spot' stiffness between our model and experiments, our results still lend some support to hypothesis (2) that metabolically costly compensation may be at play to maintain invariant net ankle moment in the face of increasing exoskeleton spring stiffness, an idea that is also corroborated by data from Collins et al. [25] indicating both local and global neuromechanical compensations during walking with parallel springs. At the ankle compensation

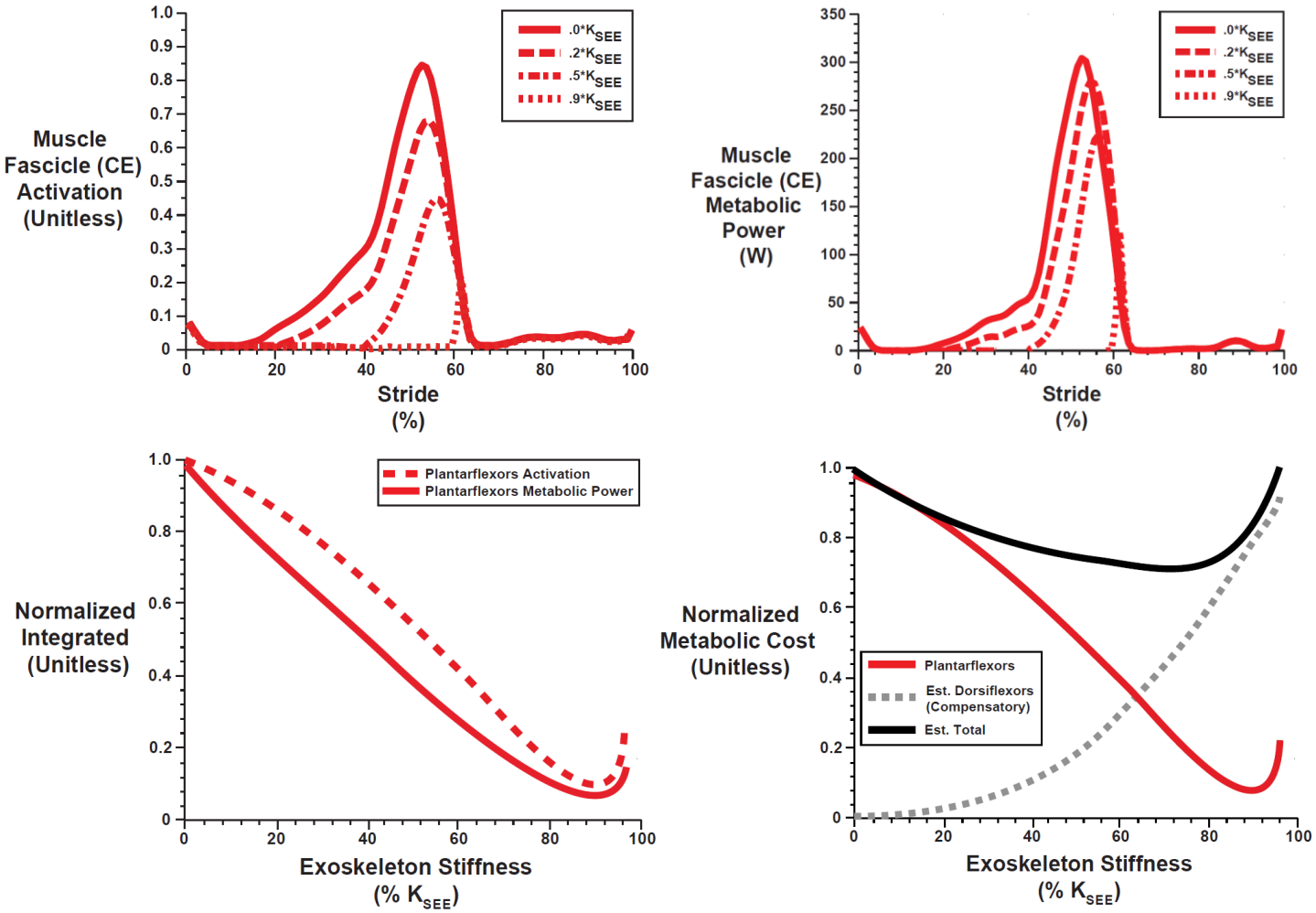

Fig. 7. (*Top*) Lumped plantarflexor muscle fascicle (CE) activation (*Top left*) and metabolic power (*Top right*) over a walking stride from heel strike (0%) to heel strike (100%) for different exoskeleton spring stiffnesses. The solid red lines represent walking without an exoskeleton (*i.e.*, the $\vec{M}_{bio}$ solution). Curves of varying line type represent exoskeleton stiffness values ranging from 0.2 K_{SEE} (~105 N-m/rad) to 0.9 K_{SEE} (~474 N-m/rad).

(*Bottom*) Integrated activation (*Left*, dashed) and metabolic power (*i.e.*, work) (*Left*, solid) versus exoskeleton spring stiffness for the lumped plantarflexor muscle fascicles (CE). Integrated metabolic power (*Right*, red) is modified (*Right*, black) to include an estimated compensatory metabolic cost (*Right*, dashed gray) due to the antagonist dorsiflexor muscle moment required to maintain an invariant net ankle moment. All values are normalized to the no exoskeleton condition. Exoskeleton spring stiffness of 100% K_{SEE} is equivalent to ~527 N-m/rad.

appears as elevated tibialis anterior muscle activity in early stance and late swing. More globally, increased knee joint moments appear near the stance-swing transition--an effect not captured by the current model.

Despite the potential for significant metabolic savings due to reduced muscle forces and activations (Figure 2, 3, 7), our results also support hypothesis (3), that elastic ankle exoskeletons could significantly disrupt the normal 'catapult action' of the plantarflexors during human walking. Our model of normal walking at 1.25 m/s (*i.e.*, K_{EXO}= 0) captures the normal muscle-tendon interaction dynamics of the plantarflexors and Achilles' tendon during walking with nearly isometric muscle fascicles during stance phase (Figure 4, bold red) and large amounts of elastic energy storage and return in series elastic tissues (Figure 5, middle, bold blue) [22, 41]. This results in a large burst of mechanical power at push-off that is shared ~50/50 between muscle fascicles (CE) and series elastic tissues (SEE) (Figure 5, 6) [22]. However, as K_{EXO} increases, unloading of the biological MTU causes less and less stretch in the SEE and more and more stretch in the CE, disrupting the normal 'catapult-like' muscle-tendon interaction (Figure 4, 5, 6).

The observation of larger CE excursions with parallel mechanical assistance is consistent with recent muscle-level experiments during spring-loaded human hopping. Soleus fascicles undergo increased excursions in the presence of a parallel spring (K_{EXO}= 91 N-m/rad) providing assistive plantarflexor torque [20]. In that case, reduced forces were counteracted by increased length changes resulting in no difference in soleus muscle fascicle work between spring-loaded and unassisted hopping conditions. Our model of spring-loaded walking makes a similar prediction that CE work does not decrease for values of K_{EXO} up to ~0.2 K_{SEE} (~ 105 N-m/rad = 1.8 N-m/deg) (Figure 6). For exoskeleton stiffness values > 0.2 K_{SEE}, CE work begins to decline as reductions in muscle force outpace increases in CE length changes. Perhaps more striking is the rapid reduction in the mechanical work performed by SEE recoil with increasing exoskeleton spring stiffness. Without assistance from the exoskeleton, the SEE recoil contributes an equal amount of mechanical power as CE shortening, but the SEE contribution is reduced to nearly zero for $K_{EXO} \geq 0.7\ K_{SEE}$ (~369 N-m/rad), completely eliminating the ability of the biological MTU to function as a catapult (Figure 6).

Increasing reliance on the CE for MTU power production limits the metabolic benefit of increasing exoskeleton spring stiffness. The lack of mechanical power from elastic recoil of the SEE is mostly supplanted by elastic recoil of the exoskeleton spring, but not without some consequence. Our metabolic cost model is driven by muscle activation, force-length and force-velocity dynamics [36] (Equations 8-11). As exoskeleton spring stiffness increases, the required muscle activation declines because biological muscle force requirements are reduced. We note, however, that reductions in metabolic cost occur at a slower rate than reductions in muscle activation (Figure 7, bottom-left). This is a direct side effect of the metabolic penalty associated with higher CE shortening velocities due to the increased muscle excursions characteristic of a disrupted 'catapult action' (Figure 4). Interestingly, because muscle fascicles nominally operate down the ascending limb (Figure 4, red bold curve), exoskeleton assistance tends to increase average fascicle lengths toward L_{CEo} , an operating point that is more favorable for force production- an effect that is trumped by far less favorable force-velocity operating points. Thus, in general, it would seem that exoskeletons designed to assist MTUs with compliant architecture may be inherently limited in their metabolic benefit. One way out of this conundrum might be for the user to adjust their joint kinematics (and therefore MTU length change pattern) in order to attenuate increases in underlying fascicle velocity that counteract the metabolic reductions due to reduced muscle forces and activations [20]. Indeed, altered joint kinematics indicative of shorter MTU lengths (*i.e.*, exaggerated plantarflexion) have been observed during walking with powered ankle orthoses [2, 29, 30] - a strategy that may limit metabolic penalty due to a disrupted 'catapult mechanism'.

Aside from improving metabolic performance of the user, exaggerated plantar flexion during walking with an ankle exoskeleton could be indicative of an injury avoidance mechanism. Although non-intuitive, walking with relatively stiff exoskeleton springs could induce passive stretch at high rates in the CE and increase the likelihood of a muscle strain injury [42]. In our simulations, the CE strain reached maximum values of ~115% for the stiffest exoskeleton spring (Figure 4), but for tasks where the MTU operates at longer lengths and/or faster velocities (*e.g.*, faster walking or walking uphill), it is possible that strains/strain rates might reach dangerous levels with relatively stiff exoskeletons (e.g. K_{EXO} > 0.9% K_{SEE} = 475 N-m/rad).

Model limitations.

We made a number of simplifications and assumptions in developing the model and simulations used in this study that are worth addressing. First and foremost, we greatly simplified the attachment geometry, muscle-tendon architecture, and mechanisms driving force production in our musculoskeletal model of the triceps surae (*i.e.*, medial gastrocnemius (MG), lateral gastrocnemius (LG) and soleus (SOL)). Briefly, we combined the triceps surae group into a single, 'lumped' uniarticular muscle-tendon with a soleus like origin and insertion locations, but with a force generating capacity of the summed MG + LG + SOL. Despite its simplicity, we believe the model captures the salient features and behaviors exhibited by the human plantar flexors during walking that are relevant to the questions we address in this study.

The inverse modeling framework we employed assumed that the overall ankle joint kinematics *and* kinetics during walking at 1.25 m/s remain invariant in the context of elastic ankle exoskeletons. While there is strong evidence that humans do indeed exhibit invariance in ankle joint moments during walking [11, 25, 29, 30], the evidence for ankle joint angle invariance is weaker. For example, Kao et al. demonstrated that, while ankle kinetics are conserved when

some plantar flexor moment is provided by a robotic exoskeleton, ankle kinematics tend to shift to more plantarflexed postures [29]. This finding has been corroborated by others who use ankle exoskeletons during human walking studies [2, 30]. We note that it is entirely possible that the devices used in previous studies were not properly 'tuned' to reproduce both ankle kinetics and kinematics during the studied gait pattern. In fact, our study strongly suggests that assistive devices that are not properly 'tuned' could lead to deviations from normal moments (Figure 3) unless the user significantly adjusts their joint kinematics and/or muscle activation patterns (Figure 7).

On the other hand, it may be that the conditions we simulated, maintaining kinematic and kinetic invariance, are not the best strategy for minimizing metabolic cost. A gait pattern with more plantarflexed posture or a higher total net plantarflexor moment may be able to better optimize the trade-off between the energy savings from reduced plantarflexor forces/muscle activations and the additional energy costs of altered movement at other places in the body (*e.g.,* knee or hip).

To address these open questions, our future work will aim toward a more complete model with more detailed anatomy and physiology that incorporates all of the individual ankle joint muscle-tendons and the rest of the lower-limb as along with an elastic ankle exoskeleton (*e.g.,* [32] for hopping) during human waking. We will use our inverse framework, but drive the simulations with actual kinematic and kinetic data from walking with elastic exoskeletons with varying spring stiffness (*e.g.,* [25]) rather than imposing invariant constraints as we did in the current study. Comparing and contrasting the fully constrained model presented here, with a model driven by 'real-world' exoskeleton walking data will provide important insights into the muscle-level mechanisms that may be guiding human preference during locomotion with exoskeleton assistance. We also plan to use ultrasound imaging to verify model predictions of underlying fascicle behavior during exoskeleton assisted walking. Indeed, a grand challenge in the field of wearable robotics is to develop a modeling and simulation framework that does not rely at *all* on imposed kinematic or kinetic constraints (from data or otherwise) to predict how walking mechanics and energetics would change in the context of novel devices.

Insights into improving current ankle exoskeleton designs.

In this study, we have highlighted a number of limitations inherent in passive elastic exoskeleton designs [8, 24] that may be overcome with improvements in future designs. The primary drawback to the device we simulated was that it produced forces too early in the stance phase that often exceeded those needed to produce a normal ankle joint moment. This effect was particularly noticeable as the exoskeleton spring stiffness increased (Figure 2, 3). With the current design, avoiding this excess exoskeleton moment would require either (a) a change in ankle joint kinematics; or (b) co-activation by ankle dorsiflexors to adjust the net ankle moment downward; or (c) walking with excessive total ankle joint moments - all of which could be considered undesirable effects. Changes in the exoskeleton design could also improve performance. For example, a passive device with non-linear spring stiffness (*i.e.,* a stiffening spring), and/or a changing moment arm could be designed with a custom torque angle curve appropriate for a given gait. In addition, timing engagement of the spring with a more versatile clutching mechanism could provide flexibility in when the exoskeleton torque onset occurs during a gait cycle. Of course, a device with motors could achieve all of the aforementioned performance features by employing customized gait-phase dependent torque control that is optimized to maximize metabolic benefit while maintaining joint kinetics and kinematics.

V. Conclusion

Our modeling results and recent experimental evidence [25] both indicate that, for devices intended to reduce metabolic cost of human locomotion by assisting compliant joints (*e.g.,* ankle), the name of the game is to reduce muscle forces and activations. This idea represents somewhat of a paradigm shift from previous solutions focusing on reducing biological muscle-tendon/ joint positive mechanical power outputs [30, 43, 44], especially in late stance phase. Passive elastic solutions are a promising alternative as they are well-suited for reducing muscle force and activation requirements in parallel biological muscle-tendon units even during periods of energy absorption [25].

Acknowledgment

We thank Glen Lichtwark and Jonas Rubenson for helpful discussions regarding the choice of model parameters, and Steve Collins for crucial feedback on the approach.

References

[1] J. Rubenson *et al.*, "On the ascent: the soleus operating length is conserved to the ascending limb of the force-length curve across gait mechanics in humans," *J Exp Biol,* vol. 215, no. Pt 20, pp. 3539-51, Oct 15, 2012.

[2] G. S. Sawicki, and D. P. Ferris, "Mechanics and energetics of level walking with powered ankle exoskeletons," *J Exp Biol,* vol. 211, no. Pt 9, pp. 1402-13, May, 2008.

[3] S. R. Ward *et al.*, "Are current measurements of lower extremity muscle architecture accurate?," *Clin Orthop Relat Res,* vol. 467, no. 4, pp. 1074-82, Apr, 2009.

[4] H. Geyer *et al.*, "Compliant leg behaviour explains basic dynamics of walking and running," *Proc Biol Sci,* vol. 273, no. 1603, pp. 2861-7, Nov 22, 2006.

[5] C. T. Farley *et al.*, "Hopping frequency in humans: a test of how springs set stride frequency in bouncing gaits," *J Appl Physiol (1985),* vol. 71, no. 6, pp. 2127-32, Dec, 1991.

[6] R. Blickhan, "The spring-mass model for running and hopping," *J Biomech,* vol. 22, no. 11-12, pp. 1217-27, 1989.

[7] T. J. Roberts, and E. Azizi, "Flexible mechanisms: the diverse roles of biological springs in vertebrate movement," *J Exp Biol,* vol. 214, no. Pt 3, pp. 353-61, Feb 1, 2011.

[8] M. B. Wiggin *et al.*, "An exoskeleton using controlled energy storage and release to aid ankle propulsion," *IEEE Int Conf Rehabil Robot,* vol. 2011, pp. 5975342, 2011.

[9] A. M. Grabowski, and H. M. Herr, "Leg exoskeleton reduces the metabolic cost of human hopping," *J Appl Physiol (1985)*, vol. 107, no. 3, pp. 670-8, Sep, 2009.

[10] D. J. Farris, and G. S. Sawicki, "Linking the mechanics and energetics of hopping with elastic ankle exoskeletons," *J Appl Physiol (1985)*, vol. 113, no. 12, pp. 1862-72, Dec 15, 2012.

[11] D. J. Bregman *et al.*, "Spring-like Ankle Foot Orthoses reduce the energy cost of walking by taking over ankle work," *Gait Posture*, vol. 35, no. 1, pp. 148-53, Jan, 2012.

[12] D. P. Ferris *et al.*, "Neuromechanical adaptation to hopping with an elastic ankle-foot orthosis," *J Appl Physiol (1985)*, vol. 100, no. 1, pp. 163-70, Jan, 2006.

[13] G. Elliott *et al.*, "The biomechanics and energetics of human running using an elastic knee exoskeleton," *IEEE Int Conf Rehabil Robot*, vol. 2013, pp. 6650418, Jun, 2013.

[14] M. S. Cherry *et al.*, "Design and fabrication of an elastic knee orthosis - preliminary results.."

[15] Y. H. Chang *et al.*, "Intralimb compensation strategy depends on the nature of joint perturbation in human hopping," *J Biomech*, vol. 41, no. 9, pp. 1832-9, 2008.

[16] E. M. Arnold *et al.*, "A model of the lower limb for analysis of human movement," *Ann Biomed Eng*, vol. 38, no. 2, pp. 269-79, Feb, 2010.

[17] G. A. Lichtwark, and A. M. Wilson, "Is Achilles tendon compliance optimised for maximum muscle efficiency during locomotion?," *J Biomech*, vol. 40, no. 8, pp. 1768-75, 2007.

[18] P. Krishnaswamy *et al.*, "Human leg model predicts ankle muscle-tendon morphology, state, roles and energetics in walking," *PLoS Comput Biol*, vol. 7, no. 3, pp. e1001107, Mar, 2011.

[19] H. Geyer, and H. Herr, "A muscle-reflex model that encodes principles of legged mechanics produces human walking dynamics and muscle activities," *IEEE Trans Neural Syst Rehabil Eng*, vol. 18, no. 3, pp. 263-73, Jun, 2010.

[20] D. J. Farris *et al.*, "Elastic ankle exoskeletons reduce soleus muscle force but not work in human hopping," *J Appl Physiol (1985)*, vol. 115, no. 5, pp. 579-85, Sep 1, 2013.

[21] D. J. Farris, and G. S. Sawicki, "The mechanics and energetics of human walking and running: a joint level perspective," *J R Soc Interface*, vol. 9, no. 66, pp. 110-8, Jan 7, 2012.

[22] D. J. Farris, and G. S. Sawicki, "Human medial gastrocnemius force-velocity behavior shifts with locomotion speed and gait," *Proc Natl Acad Sci U S A*, vol. 109, no. 3, pp. 977-82, Jan 17, 2012.

[23] J. S. Gottschall, and R. Kram, "Energy cost and muscular activity required for propulsion during walking," *J Appl Physiol (1985)*, vol. 94, no. 5, pp. 1766-72, May, 2003.

[24] M. B. Wiggin *et al.*, *Apparatus and clutch for using controlled storage and release of mechanical energy to aid locomotion*,to Google Patents, 2013.

[25] S. H. Collins *et al.*, "Reducing the energy cost of human walking using an unpowered exoskeleton," *Nature*, vol. 522, no. 7555, pp. 212-5, Jun 11, 2015.

[26] G. A. Lichtwark, and A. M. Wilson, "In vivo mechanical properties of the human Achilles tendon during one-legged hopping," *J Exp Biol*, vol. 208, no. Pt 24, pp. 4715-25, Dec, 2005.

[27] K. Albracht, and A. Arampatzis, "Exercise-induced changes in triceps surae tendon stiffness and muscle strength affect running economy in humans," *Eur J Appl Physiol*, vol. 113, no. 6, pp. 1605-15, Jun, 2013.

[28] L. Houghton *et al.*, "Achilles tendon mechanical properties after both prolonged continuous running and prolonged intermittent shuttle running in cricket batting," *J Appl Biomech*, vol. 29, no. 4, pp. 453-62, Aug, 2013.

[29] P. C. Kao *et al.*, "Invariant ankle moment patterns when walking with and without a robotic ankle exoskeleton," *J Biomech*, vol. 43, no. 2, pp. 203-9, Jan 19, 2010.

[30] P. Malcolm *et al.*, "A simple exoskeleton that assists plantarflexion can reduce the metabolic cost of human walking," *PLoS One*, vol. 8, no. 2, pp. e56137, 2013.

[31] D. J. Bregman *et al.*, "The effect of ankle foot orthosis stiffness on the energy cost of walking: a simulation study," *Clin Biomech (Bristol, Avon)*, vol. 26, no. 9, pp. 955-61, Nov, 2011.

[32] D. J. Farris *et al.*, "Musculoskeletal modelling deconstructs the paradoxical effects of elastic ankle exoskeletons on plantar-flexor mechanics & energetics during hopping," *J Exp Biol*, Oct 2, 2014.

[33] B. D. Robertson *et al.*, "More is not always better: modeling the effects of elastic exoskeleton compliance on underlying ankle muscle-tendon dynamics," *Bioinspir Biomim*, vol. 9, no. 4, pp. 046018, Dec, 2014.

[34] F. E. Zajac, "Muscle and tendon: properties, models, scaling, and application to biomechanics and motor control," *Crit Rev Biomed Eng*, vol. 17, no. 4, pp. 359-411, 1989.

[35] K. Shamaei *et al.*, "Estimation of quasi-stiffness and propulsive work of the human ankle in the stance phase of walking," *PLoS One*, vol. 8, no. 3, pp. e59935, 2013.

[36] R. M. Alexander, "Optimum muscle design for oscillatory movements," *J Theor Biol*, vol. 184, no. 3, pp. 253-59, 7 February, 1997.

[37] A. E. Minetti, and R. M. Alexander, "A theory of metabolic costs for bipedal gaits," *J Theor Biol*, vol. 186, no. 4, pp. 467-76, Jun 21, 1997.

[38] B. D. Robertson, and G. S. Sawicki, "Exploiting elasticity: Modeling the influence of neural control on mechanics and energetics of ankle muscle-tendons during human hopping," *J Theor Biol*, vol. 353, pp. 121-32, Jul 21, 2014.

[39] B. R. Umberger, and J. Rubenson, "Understanding muscle energetics in locomotion: new modeling and experimental approaches," *Exerc Sport Sci Rev*, vol. 39, no. 2, pp. 59-67, Apr, 2011.

[40] B. R. Umberger, "Stance and swing phase costs in human walking," *J R Soc Interface*, vol. 7, no. 50, pp. 1329-40, Sep 6, 2010.

[41] M. Ishikawa *et al.*, *Muscle-tendon interaction and elastic energy usage in human walking*, 2005.

[42] W. E. Garrett, Jr., "Muscle strain injuries: clinical and basic aspects," *Med Sci Sports Exerc*, vol. 22, no. 4, pp. 436-43, Aug, 1990.

[43] L. M. Mooney *et al.*, "Autonomous exoskeleton reduces metabolic cost of human walking," *J Neuroeng Rehabil*, vol. 11, pp. 151, 2014.

[44] G. S. Sawicki *et al.*, "It pays to have a spring in your step," *Exerc Sport Sci Rev*, vol. 37, no. 3, pp. 130-8, Jul, 2009.

Gregory S. Sawicki was born in Port Jefferson, New York, in 1977. He received the B.S. and M.S. degrees in mechanical engineering from Cornell University (’99) and the University of California at Davis (’01). He received the Ph.D. degree in neuromechanics (kinesiology and mechanical engineering) from the University of Michigan - Ann Arbor in 2007.

From 2007 to 2009, he was a NIH Postdoctoral Fellow in integrative biology/muscle physiology at Brown University. Since 2009, he has been on the faculty in the Joint Department of Biomedical Engineering, North Carolina State University and University of North Carolina at Chapel Hill. He directs the Human Physiology of Wearable Robotics (PoWeR) laboratory focusing on uncovering fundamental principles of locomotion mechanics, energetics and neural control in both healthy and impaired (e.g. stroke) populations. The long term vision of the Human PoWeR lab is to exploit useful principles of human locomotion- applying them to motivate bio-inspired designs for state of the art lower-limb exoskeletons prostheses.

Nabil S. Khan Nabil Khan was born in Huntsville, Alabama, in 1988. He received his B.S. in Biomedical Engineering from the University of North Carolina - Chapel Hill in 2010, and his M.S. in Biomedical Engineering from the Joint Department of Biomedical Engineering at North Carolina State University and University of North Carolina - Chapel Hill in 2013.

Since 2013, he has worked as an embedded software engineer at Anuva Innovations, Inc. in Morrisville, North Carolina. His interests include medical device development, global health engineering, and S.T.E.M. education and outreach.